Supplementary Information

Slow Magnetic Dynamics in a Centrosymmetric Didisprosium and an Equilateral Triangular Tridysprosium Molecules

Si-Guo Wu,[a] Chang-Ye Zhan,[a] Guo-Zhang Huang,[a] Ze-Yu Ruan,[a] Jun-Liang Liu*[a] and Ming-Liang Tong[a]

[a] Key Laboratory of Bioinorganic and Synthetic Chemistry of Ministry of Education, School of Chemistry, Sun Yat-Sen University, 510275 Guangzhou, Guangdong, P. R. China.

Crystal Data and Structures

Table S1. Crystallographic data and structural refinements for **1** and **2**.

Compound	**1**	**2**
Formula	$C_{124}H_{90}Cl_4Dy_2N_4O_{14}$	$C_{139}H_{115}Dy_3N_6O_{19}Cl_6$
Formula weight	2326.79	2873.59
Temperature / K	120	120
Crystal system	triclinic	trigonal
Space group	*P*-1	*R*-3
a / Å	12.3641(7)	22.1474(8)
b / Å	13.1540(8)	22.1474(8)
c / Å	16.3210(11)	45.8653(18)
α / °	94.343(2)	90
β / °	100.650(2)	90
γ / °	98.303(2)	120
V / Å^3	2567.0(3)	19483.2(16)
Z	1	6
$\rho_{calcd.}$ / g/cm^{-3}	1.505	1.302
μ / mm^{-1}	1.618	1.769
*F*000	1174.0	7662.0
Reflections collected	29360	37695
Independent reflections	11624 [R_{int} = 0.0833, R_{sigma} = 0.1131]	10729 [R_{int} = 0.0413, R_{sigma} = 0.0530]
GOF on F^2	1.035	1.073
R_1, wR_2 [$I \geq 2\sigma(I)$]^a	R_1 = 0.0587, wR_2 = 0.1285	R_1 = 0.0525, wR_2 = 0.1493
R_1, wR_2 (all data)	R_1 = 0.0948, wR_2 = 0.1438	R_1 = 0.0782, wR_2 = 0.1643
Largest diff. peak/hole / e Å^{-3}	2.11/-1.71	2.31/-1.22
CCDC No.	1978650	1978651

$^aR_1 = \sum||F_o| - |F_c||/\sum|F_o|$. $wR_2 = [\sum w(F_o^2 - F_c^2)^2/\sum w(F_o^2)^2]^{1/2}$.

Table S2. The selected bond length (Å) and bond angle (°) for **1**.

Bond length	**1**	**Bond angle**	**1**
Dy1−O1	2.253(4)	O1−Dy1−O2	86.53(14)
Dy1−O2	2.410(4)	O1−Dy1−O3	134.74(13)
Dy1−O3	2.413(4)	O1−Dy1−O4	82.63(14)
Dy1−O4	2.265(4)	O1−Dy1−O5^A	78.01(14)
Dy1−O5^A	2.390(4)	O1−Dy1−O6	133.65(12)
Dy1−O6	2.421(4)	O1−Dy1−N1	136.45(14)
Dy1−N1	2.515(4)	O1−Dy1−N2	72.24(13)
Dy1−N2	2.535(4)	O2−Dy1−O3	54.20(14)
		O2−Dy1−O6	127.38(14)
		O2−Dy1−N1	91.73(15)
		O2−Dy1−N2	79.27(14)
		O3−Dy1−O6	73.82(13)
		O3−Dy1−N1	73.07(15)
		O3−Dy1−N2	114.77(14)
		O4−Dy1−O2	160.69(14)
		O4−Dy1−O3	141.26(14)
		O4−Dy1−O5^A	114.77(13)
		O4−Dy1−O6	70.84(14)
		O4−Dy1−N1	85.27(15)
		O4−Dy1−N2	82.22(14)
		O5^A−Dy1−O2	78.21(13)
		O5^A−Dy1−O3	73.04(14)
		O5^A−Dy1−O6	79.65(13)
		O5^A−Dy1−N1	143.96(16)
		O5^A−Dy1−N2	143.46(14)
		O6−Dy1−N1	79.50(14)
		O6−Dy1−N2	136.71(13)
		N1−Dy1−N2	64.73(15)

^{A} 1-X,1-Y,1-Z.

Table S3. The selected bond length (Å) and bond angle (°) for **2**.

Bond length	**2**	**Bond angle**	**2**
Dy1–O1	2.267(3)	O1–Dy1–O2	72.49(12)
Dy1–O2	2.307(3)	O1–Dy1–O3^A	80.92(12)
Dy1–O3	2.331(3)	O1–Dy1–O3	104.85(12)
Dy1–O3	2.333(3)	O1–Dy1–O4	144.68(14)
Dy1–O4	2.372(3)	O1–Dy1–O5	85.34(14)
Dy1–O5	2.405(3)	O1–Dy1–N1^A	93.58(13)
Dy1–N1	2.554(4)	O1–Dy1–N2^A	140.36(13)
Dy1–N2	2.514(4)	O2–Dy1–O3^A	137.62(12)
		O2–Dy1–O3	81.79(12)
		O2–Dy1–O4	140.66(12)
		O2–Dy1–O5	137.69(12)
		O2–Dy1–N1^A	78.41(13)
		O2–Dy1–N2^A	70.73(14)
		O3^A–Dy1–O3	137.80(13)
		O3^A–Dy1–O4	76.29(9)
		O3–Dy1–O4	76.25(9)
		O3^A–Dy1–O5	69.47(8)
		O3–Dy1–O5	69.44(8)
		O3–Dy1–N1^A	147.40(13)
		O3^A–Dy1–N1^A	70.84(13)
		O3–Dy1–N2^A	84.10(13)
		O3^A–Dy1–N2^A	118.26(14)
		O4–Dy1–O5	61.58(17)
		O4–Dy1–N1^A	103.78(14)
		O4–Dy1–N2^A	74.84(15)
		O5–Dy1–N1^A	139.95(10)
		O5–Dy1–N2^A	132.83(14)

^{A} 1+Y-X,1-X,+Z; ^{2}1-Y,+X-Y,+Z.

Table S4. Continuous shape measures calculations (CShM)[1,2] for rare-earth ions in **1** and **2**.

Complex	**OP-8**	**HPY-8**	**HBPY-8**	**CU-8**	**SAPR-8**	**TDD-8**	**JGBF-8**
1	31.30	22.73	15.03	10.35	1.93	2.08	12.94
2	29.45	22.35	15.54	12.02	2.04	**1.62**	12.08
	JETBPY-8	**JBTPR-8**	**BTPR-8**	**JSD-8**	**TT-8**	**ETBPY-8**	
1	28.15	2.44	**1.70**	3.98	11.17	23.92	
2	27.38	2.75	2.11	3.77	12.84	22.89	

OP-8 = Octagon (D_{8h}); HPY-8 = Heptagonal pyramid (C_{7v}); HBPY-8 = Hexagonal bipyramid (D_{6h}); CU-8 = Cube (O_h); SAPR-8 = Square antiprism (D_{4d}); TDD-8 = Triangular dodecahedron (D_{2d}); JGBF-8 = J Johnson gyrobifastigium J26 (D_{2d}). JETBPY-8 = Johnson elongated triangular bipyramid J14 (D_{3h}); JBTPR-8 = Biaugmented trigonal prism J50 (C_{2v}); BTPR-8 = Biaugmented trigonal prism (C_{2v}); JSD-8 = Snub diphenoid J84 (D_{2d}); TT-8 = Triakis tetrahedron (T_d) and ETBPY-8 = Elongated trigonal bipyramid (D_{3h}).

[1] Alvarez, S.; Alemany, P.; Casanova, D.; Cirera, J.; Llunell, M.; Avnir, D. Shape maps and polyhedral interconversion paths in transition metal chemistry. *Coord. Chem. Rev.* **2005**, 249 (17), 1693-1708.

[2] Casanova, D.; Llunell, M.; Alemany, P.; Alvarez, S. The Rich Stereochemistry of Eight-Vertex Polyhedra: A Continuous Shape Measures Study. *Chem. Eur. J.* **2005**, 11 (5), 1479-1494.

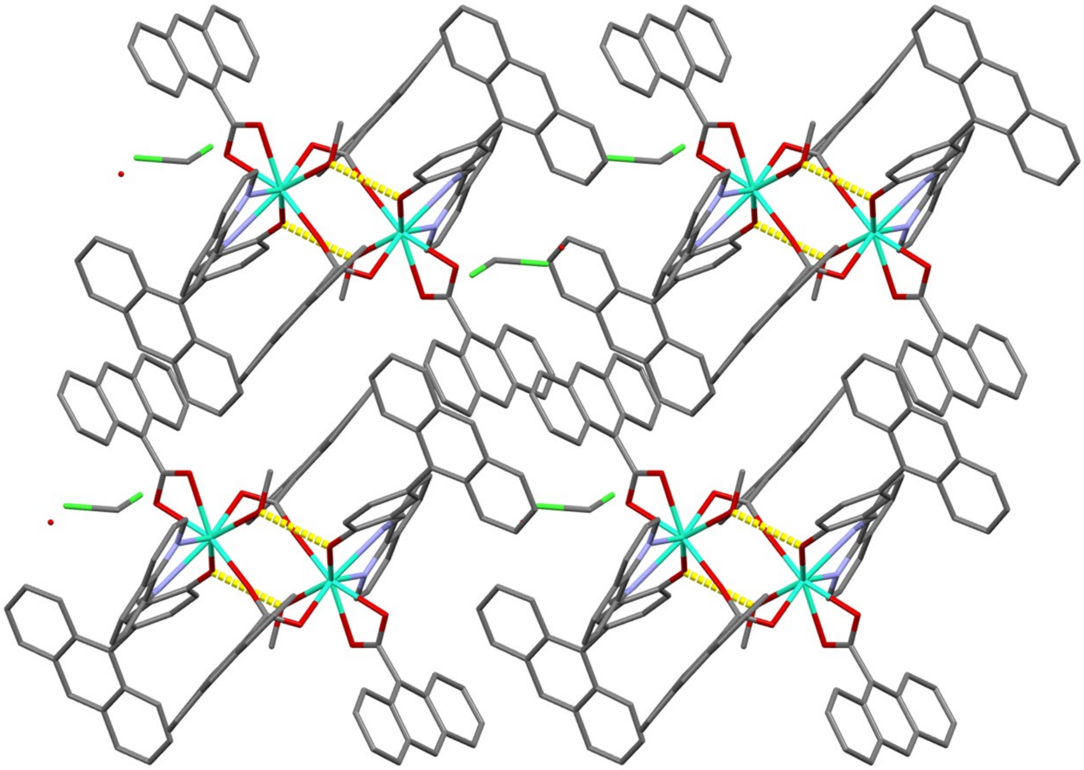

Figure S1. The packing view of **1** along *b* axis. The yellow dashed line indicates the intramolecular hydrogen bond.

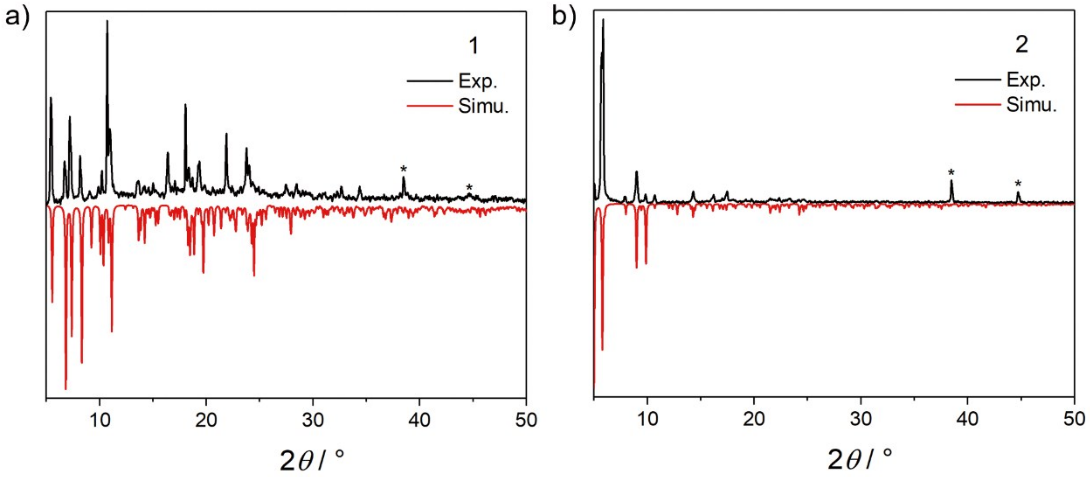

Figure S2. The experimental and simulated powder X-ray diffraction (PXRD) patterns for (a) **1** and (b) **2**. The peaks labelled with asterisks are corresponding to the sample holder. The slight offset between the experimental and the simulated patterns can be ascribed to the different measuring temperatures. The experimental data was carried out at room temperature, while the simulated pattern was from the single-crystal data identified at 120 K. The relative intensity is also influence by the crystalline shape and the grinding.

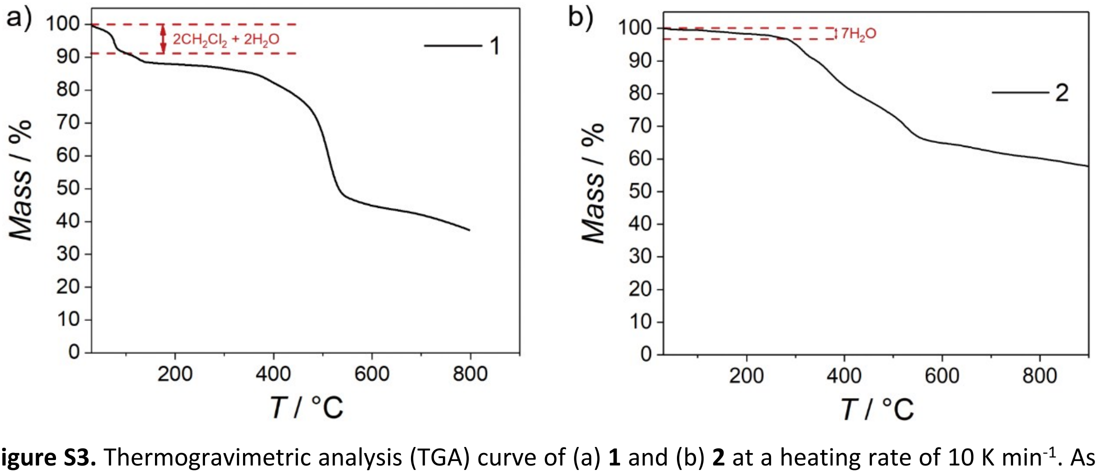

Figure S3. Thermogravimetric analysis (TGA) curve of (a) **1** and (b) **2** at a heating rate of 10 K min^{-1}. As the CH_2Cl_2 molecules in **2** escape quickly from the lattice, the air-dry sample of **2** was used in thermogravimetric measurement.

Magnetic characterization

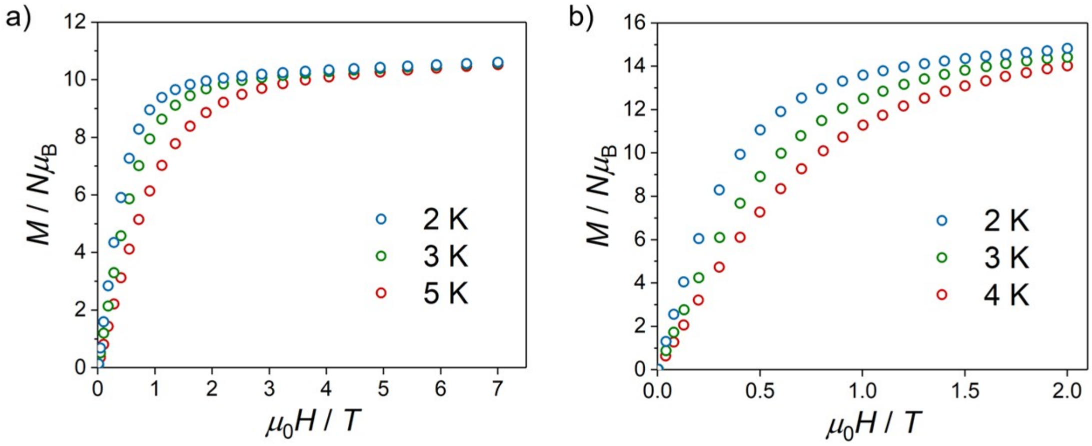

Figure S4. The filed-dependent magnetization data for (a) **1** and (b) **2**.

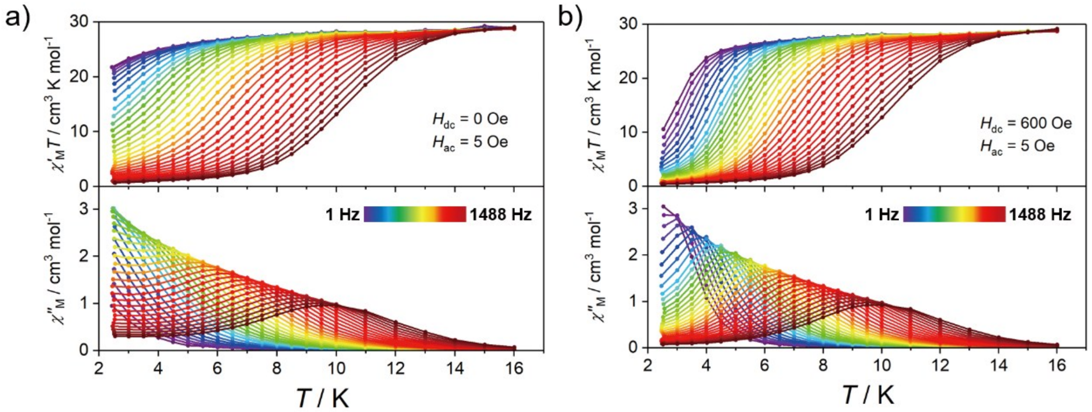

Figure S5. The temperature dependence of the in-phase (χ'_MT) and out-of-phase (χ''_M) for **1** at (a) zero dc field and (b) 600 Oe dc applied field.

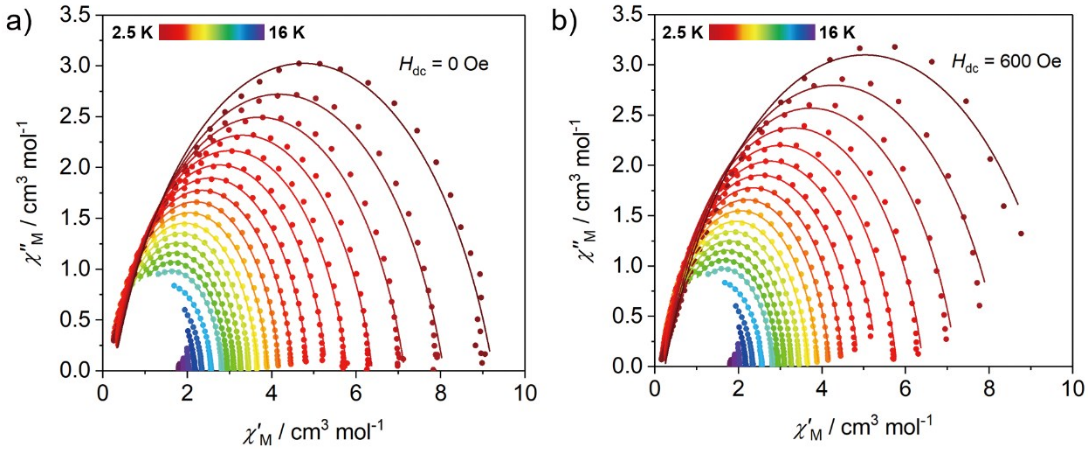

Figure S6. The Cole-Cole plots for **1** at (a) zero dc field and (b) 600 Oe dc applied field. The solid lines are fitted using a generalized Debye model.

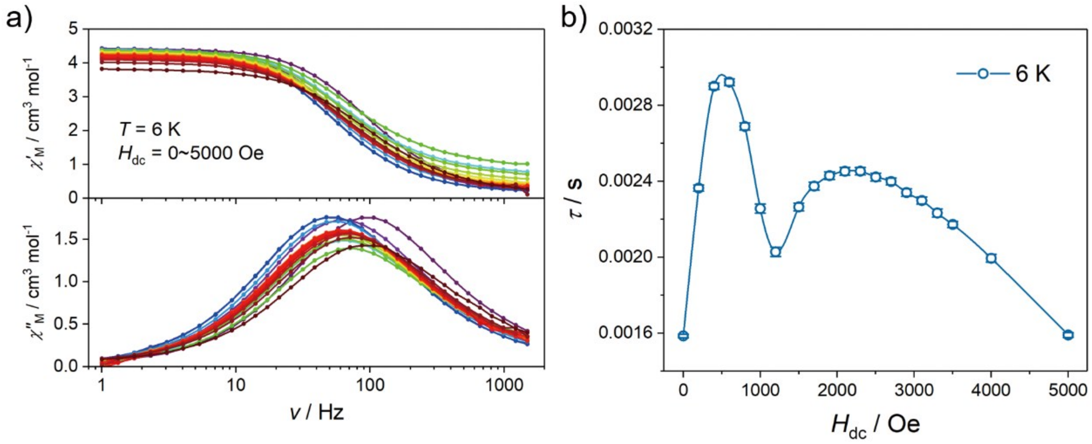

Figure S7. (a) Frequency-dependence of the in-phase product (χ'_M) and out-of-phase (χ''_M) at 6 K under 0~5 kOe dc field for **1**. (b) The relaxation time extracted from ac magnetic data at 6 K.

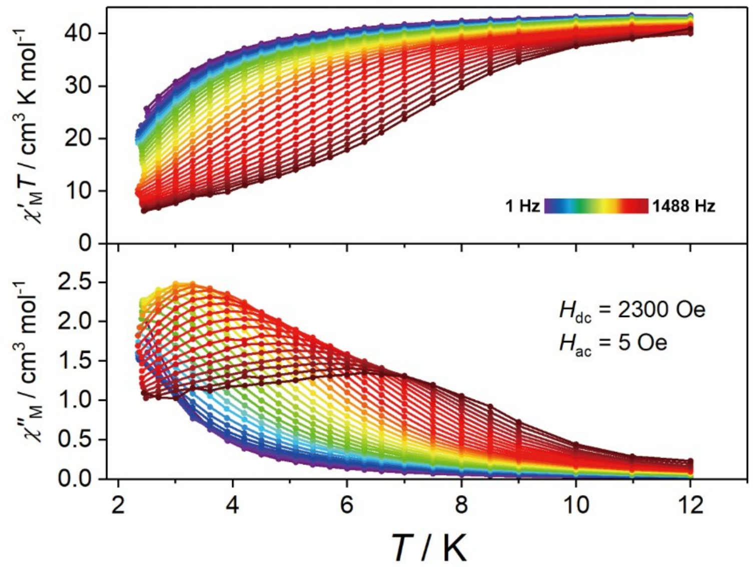

Figure S8. The temperature dependence of the in-phase ($\chi'_M T$) and out-of-phase (χ''_M) for **2** at 2300 Oe dc field.

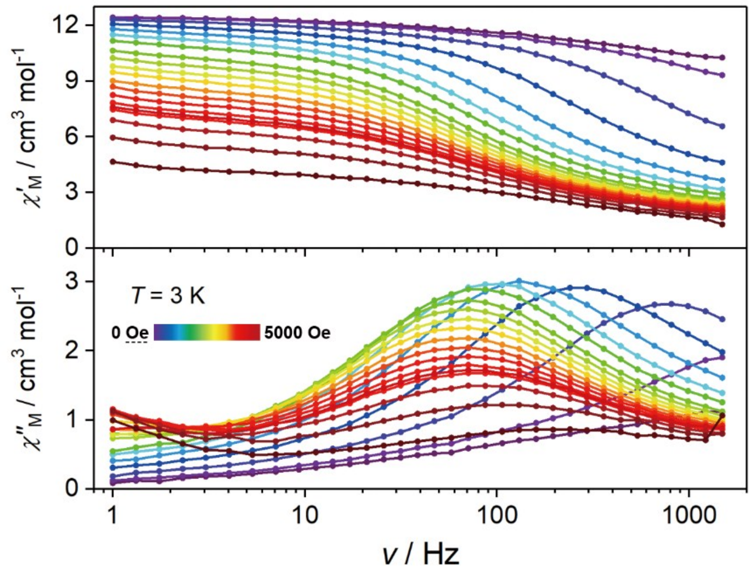

Figure S9. Frequency-dependence of the in-phase product (χ'_M) and out-of-phase (χ''_M) at 3 K under 0~5 kOe dc field for **2**.

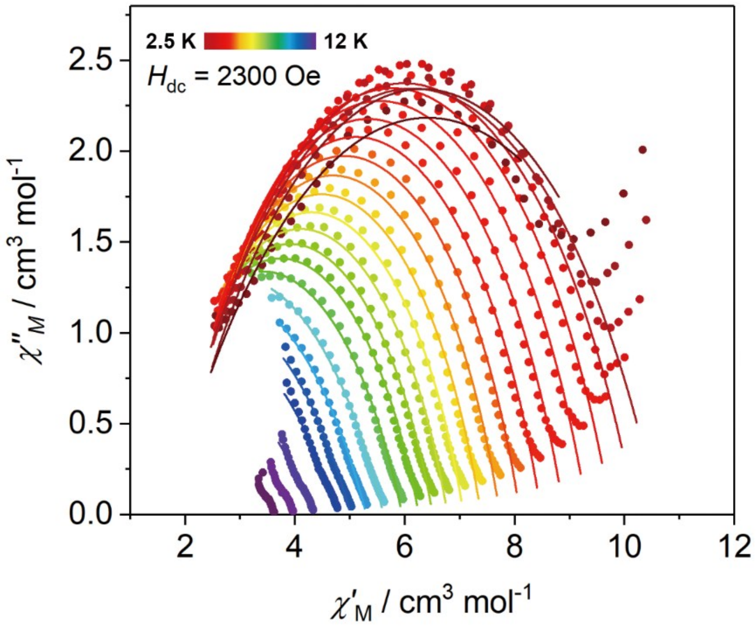

Figure S10. The Cole-Cole plots for **2** at 2300 Oe dc applied field. The solid lines are fitted using a generalized Debye model. The low-frequency region (1–10 Hz at 2.4–2.7 K) is omitted.

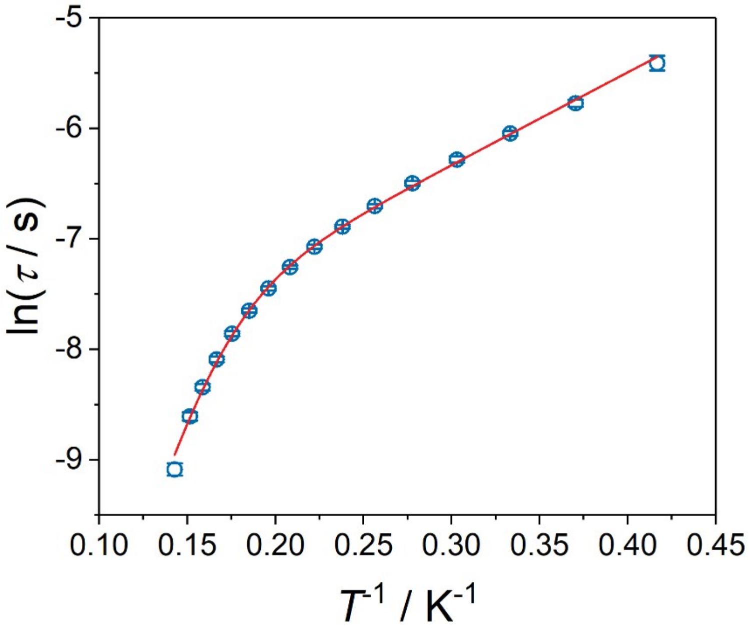

Figure S11. The relaxation time versus T plots for **2**. The red line is the best fit with equation $\tau^{-1} = \tau_{01}{}^{-1}\exp(-U_{\mathrm{eff1}}/k_BT) + \tau_{02}{}^{-1}\exp(-U_{\mathrm{eff2}}/k_BT)$ and gives U_{eff1} = 36(2) cm^{-1}, τ_{01} = 1.1(4) × 10^{-7}; U_{eff2} = 5.8(2) cm^{-1} and τ_{02} = 1.44(10) × 10^{-4} s.

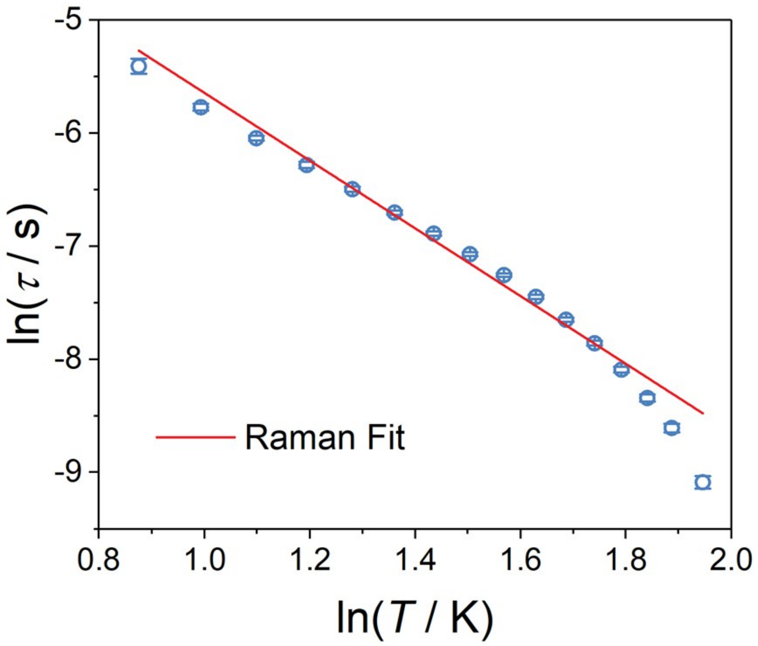

Figure S12. The relaxation time versus *T* plots for **2** in a log-log scale. The red line is the best fit with equation $\tau^{-1} = CT^n$ and gives $C = 14(1)$ s^{-1} K^{-3}, $n = 3.0(1)$.

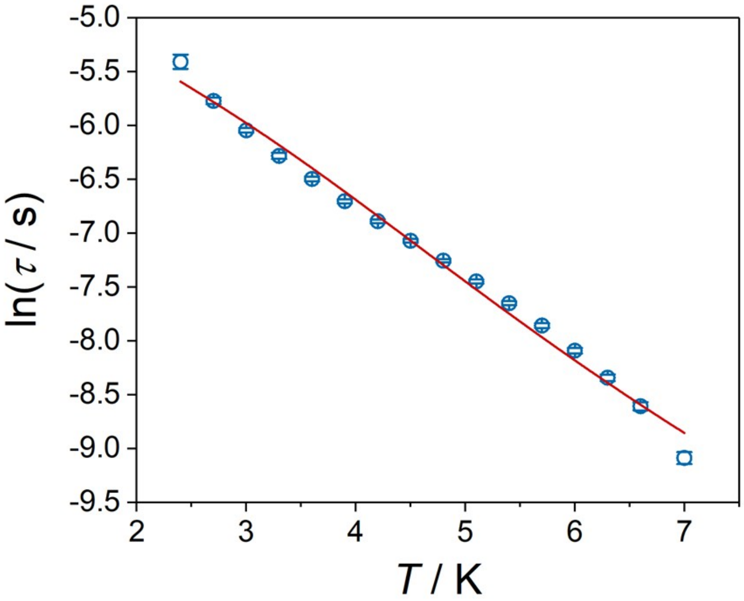

Figure S13. The relaxation time ln(τ) versus T plots for **2**. The red line is the best fit with equation $\tau^{-1} = CT^n + AT$ and gives $C = 0.5(3)$ s^{-1} K$^{-4.9}$, $n = 4.9(4)$ and $A = 97(12)$ s^{-1} K^{-1}.

Ab initio calculation

Computational Details. All *ab initio* calculations were carried out with OpenMOLCAS version 18.09[1] and are of the CASSCF/RASSI type. The Cholesky decomposition threshold was set to 1×10^{-8} to save disk space. An entire molecule was included, and the coordinates of atoms were extracted from the experimentally determined crystal structure. The neighbouring Dy(III) site was computationally replaced by the diamagnetic Y(III) for complexes **1** and **2**. ANO-RCC basis set approximations have been employed (see Table S5).[2-3] Active space of the CASSCF method included nine electrons in seven 4f orbitals of Dy(III). 21 sextets for Dy(III) were respectively optimized in state-averaged calculations and then mixed by spin−orbit coupling using RASSI approach.[4] The *g*-tensors, energies, main magnetic axis as well as the magnetizations were obtained by SINGLE_ANISO routine[5]. The magnetic interactions were fitted with PHI program[6] using Lines model[7] as in eq(1) for **1** and eq(2) for **2**, respectively.

$$\hat{H} = -2J\hat{S}_1\hat{S}_2 + \sum_{i=1,2} B_k^q \hat{O}_k^q(J_i) \tag{1}$$

$$\hat{H} = -2J\left(\hat{S}_1\hat{S}_2 + \hat{S}_2\hat{S}_3 + \hat{S}_1\hat{S}_3\right) + \sum_{i=1,2,3} B_k^q \hat{O}_k^q(J_i) \tag{2}$$

where the crystal-field parameters ($B_k{}^q$) are from the *ab initio* calculations on the Dy(III) local site (Table S8 and S9).

[1] Aquilante, F.; Autschbach, J.; Carlson, R. K.; Chibotaru, L. F.; Delcey, M. G.; De Vico, L.; Fdez. Galván, I.; Ferré, N.; Frutos, L. M.; Gagliardi, L.; Garavelli, M.; Giussani, A.; Hoyer, C. E.; Li Manni, G.; Lischka, H.; Ma, D.; Malmqvist, P. Å.; Müller, T.; Nenov, A.; Olivucci, M.; Pedersen, T. B.; Peng, D.; Plasser, F.; Pritchard, B.; Reiher, M.; Rivalta, I.; Schapiro, I.; Segarra-Martí, J.; Stenrup, M.; Truhlar, D. G.; Ungur, L.; Valentini, A.; Vancoillie, S.; Veryazov, V.; Vysotskiy, V. P.; Weingart, O.; Zapata, F.; Lindh, R. Molcas 8: New capabilities for multiconfigurational quantum chemical calculations across the periodic table. *J. Comput. Chem.* 2016, 37 (5), 506-541.

[2] Roos, B. O.; Lindh, R.; Malmqvist, P.-Å.; Veryazov, V.; Widmark, P.-O.; Borin, A. C. New Relativistic Atomic Natural Orbital Basis Sets for Lanthanide Atoms with Applications to the Ce Diatom and LuF3. *J. Phys. Chem. A* 2008, 112 (45), 11431-11435.

[3] Roos, B. O.; Lindh, R.; Malmqvist, P.-Å.; Veryazov, V.; Widmark, P.-O. Main group atoms and dimers studied with a new relativistic ANO basis set. *J. Phys. Chem. A* 2004, 108 (15), 2851-2858.

[4] Malmqvist, P. Å.; Roos, B. O.; Schimmelpfennig, B. The restricted active space (RAS) state interaction approach with spin–orbit coupling. *Chem. Phys. Lett*. 2002, 357 (3), 230-240.

[5] Chibotaru, L. F.; Ungur, L. Ab initio calculation of anisotropic magnetic properties of complexes. I. Unique definition of pseudospin Hamiltonians and their derivation. *J. Chem. Phys*. 2012, 137 (6), 064112.

[6] Chilton, N. F.; Anderson, R. P.; Turner, L. D.; Soncini, A.; Murray, K. S. PHI: a powerful new program for the analysis of anisotropic monomeric and exchange-coupled polynuclear d- and f-block complexes. *J. Comput. Chem.* 2013, *34*, 1164-1175.

[7] M. E. Lines. Orbital angular momentum in the theory of paramagnetic clusters. *J. Chem. Phys.* 1971, 55 (6), 2977-2984.

Table S5. The employed ANO-RCC basis sets for complexes **1** and **2**.

1	**2**
Dy.ANO-RCC-VTZP	Dy.ANO-RCC-VTZP
Y.ANO-RCC-VTZP	Y.ANO-RCC-VTZP
O.ANO-RCC-VDZP	O.ANO-RCC-VDZP
N.ANO-RCC-VDZP	N.ANO-RCC-VDZP
C.ANO-RCC-VDZ	C.ANO-RCC-VDZ
H.ANO-RCC-MB	H.ANO-RCC-MB

Table S6. The energy spectra and *g* tensors for the eight Kramers doublets of the ground-states of $^6H_{15/2}$ multiplets for Dy(III) ions in **1**.

E / cm^{-1}	g_x	g_y	g_z
0	0.00427	0.01637	19.58117
129.9693	0.21271	0.84679	17.92242
145.659	0.22975	0.6504	13.68975
219.6235	9.25272	7.64225	4.45123
251.9418	0.07977	2.23858	12.88587
269.1943	0.54858	2.02676	16.91733
333.4148	0.1694	0.56706	16.80884
565.6863	0.00938	0.01265	19.81747

Table S7. The energy spectra and *g* tensors for the eight Kramers doublets of the ground-states of $^6H_{15/2}$ multiplets for Dy(III) ions in **2**.

E / cm^{-1}	g_x	g_y	g_z
0	0.19906	0.58061	18.70846
41.46314	0.39113	1.01485	15.7441
102.4373	0.06625	0.85192	13.88086
144.2946	1.68512	2.77961	9.3998
190.749	3.90402	4.61492	10.3614
250.8387	1.42239	1.58437	16.03698
329.5991	0.18644	0.35261	19.38896
439.5371	0.00788	0.02475	19.69524

Table S8. The crystal-field parameters on the crystal-field splitting for the local Dy(III) sites of **1**.

k	***q***	B_k^q **(cm^{-1})**
2	-2	0.20161
2	-1	0.11845
2	0	-1.79044
2	1	-1.06673
2	2	-2.48246
4	-4	-0.0188
4	-3	-0.03485
4	-2	0.00434
4	-1	-0.0114
4	0	-0.00188
4	1	0.00819
4	2	0.00645
4	3	-0.00794
4	4	0.02657
6	-6	1.37E-04
6	-5	2.34E-04
6	-4	4.35E-05
6	-3	1.71E-04
6	-2	2.12E-04
6	-1	2.27E-04
6	0	-8.39E-06
6	1	-3.63E-05
6	2	1.25E-04
6	3	5.85E-05
6	4	-2.01E-05
6	5	-5.37E-06
6	6	-1.11E-04

$\hat{H} = \sum B_k^q \hat{O}_k^q$, where $\hat{O}_k^q$ is the extended Steven operators.

Table S9. The crystal-field parameters on the crystal-field splitting for the local Dy(III) sites of **2**.

k	q	B_k^q (cm^{-1})
2	-2	0.67115
2	-1	2.01597
2	0	-1.48991
2	1	0.52674
2	2	0.62054
4	-4	0.01437
4	-3	0.11202
4	-2	0.00134
4	-1	-0.00858
4	0	-9.57E-04
4	1	6.50E-04
4	2	0.01704
4	3	0.00962
4	4	-0.01956
6	-6	1.78E-04
6	-5	9.61E-05
6	-4	1.25E-04
6	-3	-3.15E-04
6	-2	1.27E-06
6	-1	-6.61E-05
6	0	1.01E-05
6	1	1.92E-05
6	2	-1.23E-05
6	3	1.18E-04
6	4	-1.08E-04
6	5	-6.12E-04
6	6	-3.86E-05

$\hat{H} = \sum B_k^q \hat{O}_k^q$, where $\hat{O}_k^q$ is the extended Steven operators.

Table S10. Energies (cm^{-1}) of the 2 lowest exchange doublets for complex **1** and the 4 lowest exchange doublets for complex **2**.

KD (Complex **1**)	E (cm^{-1})	**KD** (Complex **2**)	E (cm^{-1})
1	0	**1**	0
2	0.5698	**2**	0.2407
		3	0.2410
		4	0.2410